

Journal of Biomedical Optics

BiomedicalOptics.SPIEDigitalLibrary.org

Raman microspectroscopy of nanodiamond-induced structural changes in albumin

Anastasiya S. Svetlakova
Nikolay N. Brandt
Alexander V. Priezzhev
Andrey Yu. Chikishev

Raman microspectroscopy of nanodiamond-induced structural changes in albumin

Anastasiya S. Svetlakova,^{a,*} Nikolay N. Brandt,^a Alexander V. Priezzhev,^{a,b} and Andrey Yu. Chikishev^b

^aLomonosov Moscow State University, Physics Department, Leninskie Gory 1/62, Moscow 119991, Russia

^bLomonosov Moscow State University, International Laser Center, Leninskie Gory 1/62, Moscow 119992, Russia

Abstract. Nanodiamonds (NDs) are promising agents for theranostic applications due to reported low toxicity and high biocompatibility, which is still being extensively tested on cellular, tissue, and organism levels. It is presumed that for experimental and future clinical applications, NDs will be administered into the organism via the blood circulation system. In this regard, the interaction of NDs with blood components needs to be thoroughly studied. We studied the interaction of carboxylated NDs (cNDs) with albumin, one of the major proteins of blood plasma. After 2-h long *in vitro* incubation in an aqueous solution of the protein, 100-nm cNDs were dried and the dry samples were studied with the aid of Raman microspectroscopy. The spectroscopic data indicate significant conformational changes that can be due to cND–protein interaction. A possible decrease in the functional activity of albumin related to the conformational changes must be taken into account in the *in vivo* applications. © 2015 Society of Photo-Optical Instrumentation Engineers (SPIE) [DOI: 10.1117/1.JBO.20.4.047004]

Keywords: Raman microspectroscopy; nanodiamonds; protein structure; albumin.

Paper 140695RR received Oct. 22, 2014; accepted for publication Mar. 30, 2015; published online Apr. 22, 2015.

1 Introduction

Nanoparticles are promising for applications in biotechnology and theranostics since they can be used for addressed drug delivery and visualization of various processes in living organisms. Nanoparticles and their conjugates with drugs can be administered and spread via the blood circulation system. In this regard, it is expedient to study the interaction of nanoparticles with tissues and blood components within the framework of the problems of nanotoxicology and nanosafety. It is known that the nanoparticles are sometimes able to induce dramatic effects on protein interactions.¹ The general use of nanoparticles in nanomedicine has been reviewed in multiple works (see, e.g., Refs. 2–4).

Diamond nanoparticles, nanodiamonds (NDs), exhibit high biocompatibility and relatively low toxicity,⁵ their properties can be characterized using fluorescence and Raman spectroscopy,⁶ and the corresponding signals can be used for ND visualization.^{7–9} The bioconjugation can be facilitated with the aid of functionalization of the ND surface (e.g., by means of carboxylation).^{10–12} The absence of toxicity of carboxylated NDs (cNDs) has been demonstrated in Refs. 8 and 13 for *in vitro* interaction with various cells of human organisms. However, several experiments with *in vivo* and *in vitro* incubations have shown that NDs are accumulated in internal organs of laboratory animals (rats)¹⁴ and can stick to the membranes and penetrate into erythrocytes.¹⁵ In the tested range of particle concentrations, such an interaction did not cause hemolysis of the cells but potentially it may affect their microrheologic properties (reversible aggregation and deformability).¹⁵

It is known that the proteins of blood plasma are adsorbed on the ND surface.^{16–18} FTIR data show that the interaction of

human serum albumin (HSA) and cNDs with linear sizes of 5 and 100 nm leads to the changes of the amide I band shape and variations in the relative intensities of amide I–III bands, which indicate variations in the protein secondary structure.¹⁹

The results of Ref. 20 show a minor increase in the relative contents of random coils and β -sheets upon the dominant contribution of α -helices to the secondary structure of bovine serum albumin (BSA) that forms a complex with 5-nm cNDs. In addition, the complex formation leads to a minor blue shift of the UV-VIS absorption band of the protein and significant quenching of the protein fluorescence.

Lysozyme binding with 100-nm cND results in the splitting and low-frequency shifting of the band at 3250 cm^{-1} (N–H stretching) in the FTIR spectra.^{21,22} In this case, the enzymatic activity remains almost unchanged. The interaction with 5-nm cNDs also leads to the low-frequency shifting and splitting of the band into three narrow bands. The FTIR spectra of lysozyme^{19,23} show a high-frequency shift of the amide I band due to complex formation with cNDs. The shifts for 5- and 50-nm cNDs are greater than the shift for the 100-nm cNDs. The relative contents of random coils and β -sheets slightly increase in the predominantly α -helical protein. The enzymatic activity of lysozyme decreases by 80%, 80%, 25%, and 40% in complexes with 5-, 50-, 100-, and 500-nm cNDs, respectively.

However, the results of Ref. 24 show that the adsorption of blood plasma on NDs does not lead to variations in the secondary structure of the blood-plasma proteins and that incubation with NDs does not affect the dynamics of blood coagulation.

Thus, the existing data indicate the interaction of blood-plasma proteins and NDs; however, the nature and result of such interaction remain unclear and a conclusion on variations

*Address all correspondence to: Anastasiya S. Svetlakova, E-mail: svetlakova.anastasiya@physics.msu.ru

in the protein structure due to adsorption on ND surface is not commonly accepted. Biofunctionalization of nanoparticles involves the functional activity of protein molecules bound to the surface of a nanoparticle. Hence, it is expedient to learn more about the effects of the interaction with ND on the structure and function of proteins.

In this work, we employed Raman microspectroscopy to study the conformational changes of albumin that were induced by the interaction with NDs. Raman microspectroscopy is an efficient tool in the study of the structure of various biological objects.^{25–28} Raman spectra of proteins exhibit several conformation-sensitive bands: amide I ($\sim 1640\text{ cm}^{-1}$), amide III ($\sim 1270\text{ cm}^{-1}$), tyrosine doublet (830 and 855 cm^{-1}), bands of the disulfide bridges (510 , 525 , and 540 cm^{-1}), and several bands assigned to the vibrations of tryptophan residues (e.g., 1361 cm^{-1}).²⁹

2 Samples and Methods

In the experiments, we used BSA from MP Biomedicals (CAS #9048-46-8) ($M_{\text{BSA}} 66.3\text{ kD}$), HSA from Sigma Aldrich (CAS #70024-90-7) ($M_{\text{HSA}} 66.2\text{ kD}$), and NDs from Kay Industrial Diamond. The NDs with a characteristic size of about 100 nm were carboxylated using a mixture of sulfuric and nitric acids (3:1). The characteristic size of a single ND is approximately 20 times greater than the characteristic linear size of an HSA molecule.

To prepare a buffer solution, we sequentially dissolved sodium chloride (4 g), potassium chloride (0.72 g), orthophosphoric acid (0.72 g), and potassium dihydrogen phosphate (0.12 g) in deionized distilled water (500 ml). The buffer pH (7.4) was equal to the mean pH of human blood. The buffer was sterilized and stored at a temperature of 4°C . Carboxylated NDs (cNDs) were added to the HSA solution in buffer: the concentrations were 2 and 20 mg/ml , respectively. Ultrasonic processing was used to destroy cND aggregates, and the resulting suspension was stored in a shaker over 2 h . Then the following procedure was repeated three times: the suspension (1 mL) was centrifuged at $11,000g$ during 10 min to provide precipitation of cNDs with adsorbed protein molecules, the supernatant fluid ($950\text{ }\mu\text{L}$) was removed, and the buffer (1 mL) was added. In each cycle, the absorption spectrum of the

supernatant fluid was measured. At the last stage, the buffer was not added. The resulting cND-HSA samples ($20\text{ }\mu\text{L}$) were deposited on a silicon substrate and dried at room temperature.

A reference buffer solution of HSA with a concentration of 20 mg/mL was processed using a similar procedure and dried at room temperature on a silicon substrate.

Tris-2-carboxyethyl phosphine (TCEP) was used as a chemical agent that provides the cleavage of disulfide bonds.³⁰ To prepare the TCEP-HSA sample, we used an aqueous (Milli-Q) solution of HSA (7.6 mg/mL) and TCEP (0.55 mg/ml) in which the TCEP-to-protein molar ratio was $17:1$. The solution was processed in an ultrasonic bath over 30 min and stored at room temperature over 2 h . Then the sample was lyophilized. A reference HSA sample was prepared using the same procedure.

For the Raman measurements, we used a Thermo Scientific DXR Raman confocal microscope. The excitation wavelength was 532 nm , the mean power at the sample was no greater than 10 mW , and the spectral resolution was 5 cm^{-1} (the dispersion was about $1\text{ cm}^{-1}/\text{pixel}$). The diameters of the focal spots on the sample and the confocal resolution were 0.6 and $4\text{ }\mu\text{m}$, respectively ($100\times$ objective and $25\text{-}\mu\text{m}$ pinhole). Raman bands were assigned using the results of Refs. 29 and 31–33.

3 Results and Discussion

Optical microscopy shows that the cND-HSA samples under study consist of irregularly shaped microstructures. Figure 1(a) presents a typical microphotograph of a dried cND-HSA sample. It is clearly seen that the sample consists of microstructures that apparently represent the aggregates of protein molecules and cNDs. To estimate the characteristic size of the microstructures, we used ImageJ software. Figure 1(b) shows the resulting size distribution with a mean linear size of about $3\text{ }\mu\text{m}$. Note that most microstructures on the surface of the samples are in close contact with each other, and the thickness of the sample exceeds the size of the microstructures. Therefore, obtaining the real size distribution of microstructures is not feasible.

We measured the Raman spectra at 100 randomly located microstructures to assess their identity. Based on the spectral

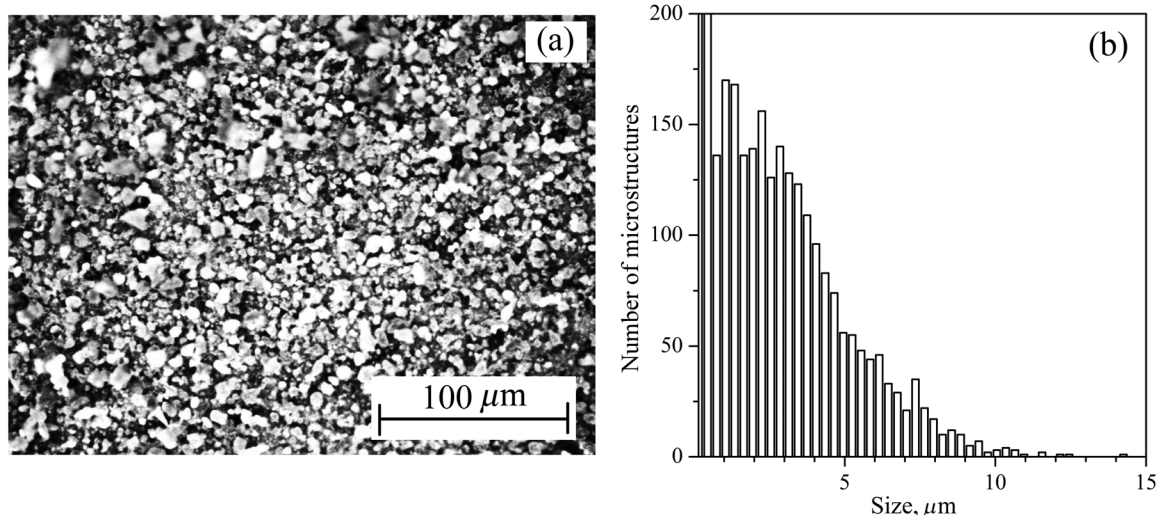


Fig. 1 (a) Microphotograph of a surface fragment of cND-HSA sample dried on silicon substrate and (b) distribution of microstructures with respect to their size.

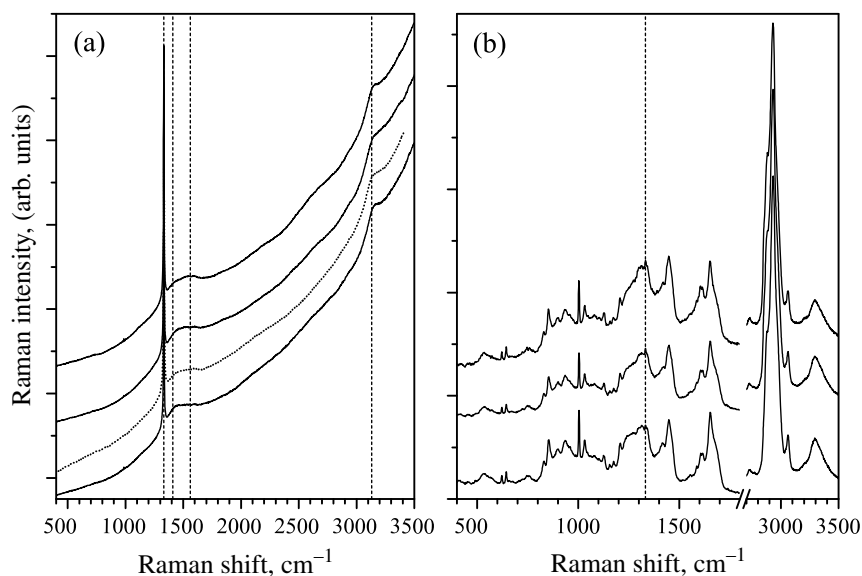


Fig. 2 Raman spectrum of cND sample (dotted line). Solid lines show Raman spectra of cND-HSA sample measured at several sites on its surface that are classified as the spectra of (a) diamond and (b) protein. The dashed lines show the positions of the Raman bands at 1332, 1410, 1560, and 3130 cm^{-1} (see text for details).

data, we conclude that most microstructures predominantly consist of cNDs [Fig. 2(a)]: an intense narrow band at 1332 cm^{-1} is assigned to diamond (vibrations of carbon in sp^3 hybridization), overlapped broadbands at 1410 and 1560 cm^{-1} are assigned to defect and ordered graphites, respectively (D and G graphite bands), and the band at 3130 cm^{-1} corresponds to the C–H stretching mode.⁶ Note the absence of Raman signatures of proteins in these spectra, which, however, does not exclude the presence of small amounts of protein molecules.

The measurements at two microstructures of 100 yielded the spectra that can be identified as the Raman spectra of protein with a contribution of the diamond band at 1332 cm^{-1} . The spectra were measured at five sites on each microstructure. In these 10 almost identical spectra [Fig. 2(b) shows three of them], we observe the protein bands at about 540 cm^{-1} (vibrations of disulfide bridges), 830 and 850 cm^{-1} (tyrosine doublet), 1006 cm^{-1} (breathing mode of phenylalanine ring), and 1640 cm^{-1} (amide I). The bands assigned to the C–H and N–H stretching modes are observed at ~ 2900 and ~ 3300 cm^{-1} , respectively.

Below, we consider the Raman spectrum of one of the cND-HSA samples that results from averaging the above 10 measurements.

Figure 3 shows the Raman spectra of the reference HSA and cND-HSA samples. Background signals were subtracted using the method described elsewhere,³⁴ and the resulting spectra were normalized by the intensity of the band at 2930 cm^{-1} (C–H stretching mode).

It is seen that the intensities of the bands at 510 and 670 cm^{-1} are significantly lower in the spectrum of the cND-HSA sample. The bands in the interval 500 to 550 cm^{-1} are assigned to S–S stretching vibrations. C–S stretching vibrations are manifested at 660 to 670 and 700 cm^{-1} in C–S–S–C and C–S–C configurations, respectively.³¹ The Protein Data Bank (PDB) data for HSA show that the protein structure contains 17 disulfide bridges, 34 C–S bonds in C–S–S–C configuration, 6 C–S bonds in C–S–C configuration, and 1 C–S bond in

C–S–H configuration. Thus, a decrease in the intensities of the bands at 510 and 675 cm^{-1} can be due to the cleavage of disulfide bonds and the corresponding decrease in the number of C–S bonds in C–S–S–C configuration. To prove such an interpretation, we additionally studied the mixture of HSA with TCEP. The inset to Fig. 3 compares the Raman spectra of lyophilized HSA and TCEP-HSA samples and shows that the cleavage of disulfide bonds leads to a decrease in the intensities of the bands at 510 and 670 cm^{-1} . Such spectral changes are similar to the spectral changes for cND-HSA samples.

For cND-HSA samples, we also observe an increase in the intensity ratio of tyrosine doublet $R = I_{850}/I_{830}$, which characterizes the H-bonding of tyrosine residues, from $R = 1.4$ for HSA to $R = 2.1$ for cND-HSA. Based on the existing data,

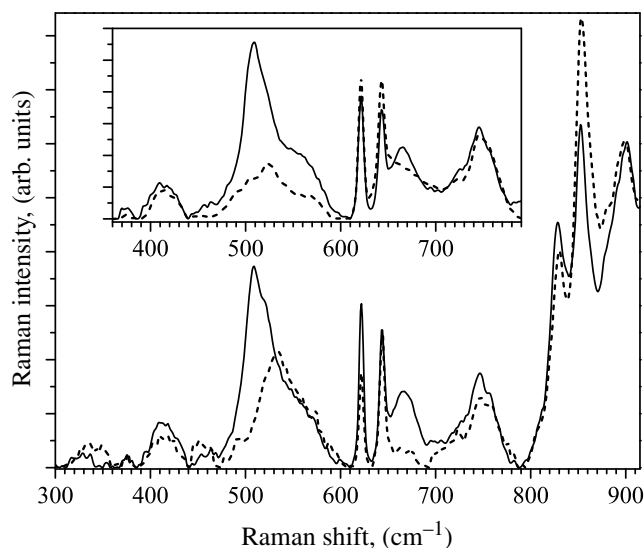


Fig. 3 Raman spectra of reference HSA sample (solid line) and cND-HSA sample (dashed line). The inset shows Raman spectra of lyophilized HSA (solid line) and TCEP-HSA samples (dashed line).

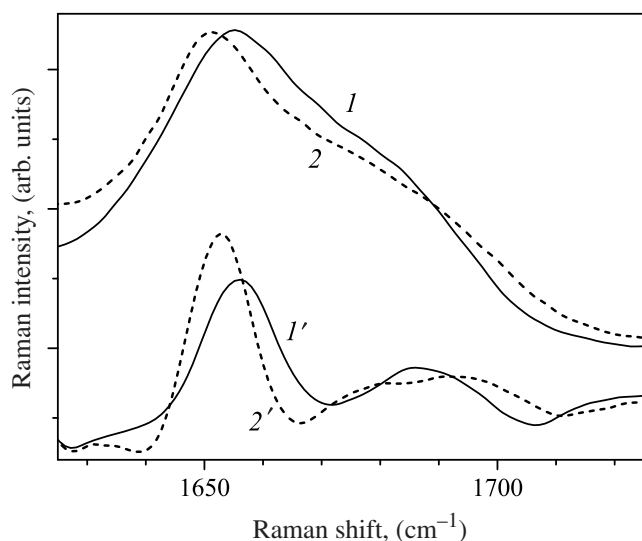


Fig. 4 Raman spectra of reference HSA (1) and cND-HSA samples (2) and second derivatives of the corresponding spectra (1') and (2').

we conclude that OH groups of tyrosine residues become stronger acceptors in H-bonds.

We additionally measured the Raman spectra of cND-protein samples in which BSA was used instead of HSA. The spectra of 100 microstructures were measured. The protein spectrum was observed for only one microstructure. The measurements at 10 points at this microstructure yielded a decrease in the intensities of the bands at 510 and 670 cm^{-1} and a variation in *R*-ratio as well as the measurements with HSA did.

To compare the shapes of amide I bands, we preliminary subtracted linear backgrounds and normalized the resulting spectra by the integrals over the spectral interval 1640 to 1720 cm^{-1} (curves 1 and 2, Fig. 4). We also used the double differentiation of the spectra (curves 1' and 2', Fig. 4). Note an increase in the intensity at 1650 cm^{-1} and a decrease in the intensity at 1660 to 1670 cm^{-1} in the spectrum of the cND-HSA sample. In accordance with PDB data, the relative contents of the main elements of the secondary structure (alpha-helix, beta-sheet, and random coil) are 78%, 0%, and 22%, respectively.³⁵ Alpha-helices and random coils predominantly contribute to the spectral intensities in the intervals 1650 to 1657 and 1660 to 1665 cm^{-1} , respectively.^{29,36–38} Therefore, the experimental results show that the relative content of alpha-helices (random coils) increases (decreases) in the cND-HSA samples.

The absence of Raman signatures of protein in the spectra of most microstructures is an unexpected result. Estimations based on the initial concentrations of cNDs and HSA and the concentrations of protein in supernatant fluids after centrifuging (results of spectrophotometric measurements) show that about 10,000 protein molecules are bound to a single cND. The resulting sample under study must contain a significant amount of bounded protein molecules (the protein mass in the sample is estimated to be 1.5 mg). In a test experiment, we measured the Raman spectra of lyophilized HSA pressed in a tablet with a mass of 1.5 mg and an area of about 20 mm^2 . The measurements at several points on such a sample yielded identical signal levels that were no less than the signal levels at the points where the protein was detected in the experiments with cND-HSA samples. Thus, the fact that the Raman signal of protein is difficult to detect in cND-HSA samples disagrees with a

relatively high amount of protein in the sample under study. We may assume that cNDs form microstructures with encapsulated protein molecules, so that the latter becomes undetectable in Raman measurements. A minor part of such microstructures can be destroyed in the course of the sample preparation. Protein molecules at such locations are liberated and exposed to laser excitation, therefore, the Raman spectrum of protein can be measured. This speculation needs to be verified in additional experiments.

4 Conclusion

The cND-HSA dried samples are structurally nonuniform and consist of microstructures. Few areas with relatively high concentrations of protein molecules are detected although the estimations show that the total amount of protein molecules in the sample under study is sufficient for reliable detection at any point of the sample under the conditions for uniform distribution.

The spectral data indicate the following conformational changes of protein molecules induced by the interaction with cNDs: cleavage of disulfide bridges, modifications of H-bonds of tyrosine residues, and a minor increase (decrease) in the relative content of α -helices (random coils).

Such significant conformational changes of HSA in the cND-HSA complex may lead to a decrease in the functional activity of protein molecules bound to the surface of cNDs. In respect to the effect of the alteration of the functional activity of HSA on the biofunctionalization of cND for drug delivery, it should be noted that the altered structure and functional activity of albumin may impede the functionalization needed for attaching the drug to the nanoparticle. Thus, the addressed drug delivery with the aid of cNDs that are biofunctionalized using HSA molecules may be inefficient. However, the system under study was obtained under conditions that substantially differ from *in vivo* conditions. In native medium, the cND-HSA interaction can be different, so this interaction in aqueous medium should be additionally studied in more detail.

Acknowledgments

We are grateful to IR Laboratory of National Dong Hwa University, Taiwan for providing cNDs. This work was supported in part by the Russian Foundation for Basic Research (Grant Nos. 12-02-92008, 13-02-01177, and 15-02-06512) and Lomonosov Moscow State University Development Program.

References

1. I. Lynch and K. A. Dawson, "Protein-nanoparticle interactions," *Nanotoday* **3**, 40–47 (2008).
2. M. L. Etheridge et al., "The big picture on nanomedicine: the state of investigational and approved nanomedicine products," *Nanomedicine* **9**, 1–14 (2013).
3. Y. Xing and L. Dai, "Nanodiamonds for nanomedicine," *Nanomedicine* **4**, 207–218 (2009).
4. D. Ho, *Nanodiamonds: Applications in Biology and Medicine*, Springer-Verlag, USA (2010).
5. S. J. Yu et al., "Bright fluorescent nanodiamonds: no photobleaching and low cytotoxicity," *J. Am. Chem. Soc.* **127**(50), 17604–17605 (2005).
6. V. N. Mochalin et al., "The properties and applications of nanodiamonds," *Nat. Nanotechnol.* **7**, 11–23 (2011).
7. T. C. Hsu et al., "Labeling of neuronal differentiation and neuron cells with biocompatible fluorescent nanodiamonds," *Sci. Rep.* **4**, 5004 (2014).

8. K. K. Liu et al., "Biocompatible and detectable carboxylated nanodiamond on human cell," *Nanotechnology* **18**, 325102 (2007).
9. C.-Y. Cheng et al., "Direct and *in vitro* observation of growth hormone receptor molecules in A549 human lung epithelial cells by nanodiamond labeling," *Appl. Phys. Lett.* **90**(16), 163903 (2007).
10. J. T. Paci et al., "Understanding the surfaces of nanodiamonds," *J. Phys. Chem.* **117**, 17256–17267 (2013).
11. K.-K. Liu et al., "Biocompatible and detectable carboxylated nanodiamond on human cell," *Nanotechnology* **18**, 1–11 (2007).
12. V. Paget et al., "Carboxylated nanodiamonds are neither cytotoxic nor genotoxic on liver, kidney, intestine and lung human cell lines," *Nanotoxicology* **8**, 46–56 (2014).
13. V. Paget et al., "Carboxylated nanodiamonds are neither cytotoxic nor genotoxic on liver, kidney, intestine and lung human cell lines," *Nanotoxicology* **8**(S1), 46–56 (2014).
14. Y. Yuan et al., "Biodistribution and fate of nanodiamonds *in vivo*," *Diamond Relat. Mater.* **18**, 95–100 (2009).
15. Y.-C. Lin et al., "The influence of nanodiamond on the oxygenation states and micro rheological properties of human red blood cells *in vitro*," *J. Biomed. Opt.* **17**(10), 1015121 (2012).
16. X. L. Kong et al., "High-affinity capture of proteins by diamond nanoparticles for mass spectrometric analysis," *Anal. Chem.* **77**(1), 259–265 (2005).
17. L.-C. L. Huang and H.-C. Chang, "Adsorption and immobilization of cytochrome c on nanodiamonds," *Langmuir* **20**(14), 5879–5884 (2004).
18. V. S. Bondar, I. O. Pozdnyakova, and A. P. Puzyr, "Applications of nanodiamonds for separation and purification of proteins," *Phys. Solid State* **46**(4), 758–760 (2004).
19. E. V. Perevedentseva et al., "Laser-optical investigation of the effect of diamond nanoparticles on the structure and functional properties of proteins," *Quantum Electron.* **40**(12), 1089–1093 (2011).
20. H. D. Wang et al., "Study on protein conformation and adsorption behaviors in nanodiamond particle-protein complexes," *Nanotechnology* **22**, 145703 (2011).
21. E. V. Perevedentseva et al., "The interaction of protein-modified nanodiamond with bacterial cells," *Nanotechnology* **2**, 440–443 (2006).
22. P.-H. Chung et al., "Spectroscopic study of bio-functionalized nanodiamonds," *Diamond Relat. Mater.* **15**, 622–625 (2006).
23. E. V. Perevedentseva et al., "Characterizing protein activities on the lysozyme and nanodiamond complex prepared for bio applications," *Langmuir* **27**(3), 1085–1091 (2011).
24. J. Mona et al., "Adsorption of human blood plasma on nanodiamond and its influence on activated partial thromboplastin time," *Diamond Relat. Mater.* **39**, 73–77 (2013).
25. Q. Tu and C. Chang, "Diagnostic applications of Raman spectroscopy," *Nanomedicine* **8**, 545–558 (2012).
26. J. Popp, C. Krafft, and T. Mayerhofer, "Modern Raman spectroscopy for biomedical applications," *Opt. Photonik* **6**(4), 24–28 (2011).
27. H. U. Gremlich and B. Yan, *Infrared and Raman Spectroscopy of Biological Materials*, Marcel-Dekker, New York (2001).
28. E. B. Hanlon et al., "Prospects for *in vivo* Raman spectroscopy" *Phys. Med. Biol.* **45**, R1–R59 (2000).
29. I. N. Serdyuk, N. R. Zaccai, and J. Zaccai, *Methods in Molecular Biophysics: Structure, Dynamics, Function*, Cambridge University Press, Cambridge/New York/Melbourne (2007).
30. C. David, S. Foley, and M. Enescu, "Protein S–S bridge reduction: a Raman and computational study of lysozyme interaction with TCEP," *Phys. Chem. Chem. Phys.* **11**, 2532–2542 (2009).
31. R. C. Lord and N.-T. Yu, "Laser-excited Raman spectroscopy of biomolecules. I. Native lysozyme and its constituent amino acids," *J. Mol. Biol.* **50**(2), 509–524 (1970).
32. H. Li et al., "Determination of the pKa values of active-center cysteines, cysteines-32 and -35, in *Escherichia coli* thioredoxin by Raman spectroscopy," *Biochemistry* **32**(22), 5800–5808 (1993).
33. R. C. Lord and N.-T. Yu, "Laser-excited Raman spectroscopy of biomolecules II. Native ribonuclease and α -chymotrypsin," *J. Mol. Biol.* **51**, 203–213 (1970).
34. I. K. Mikhailyuk and A. P. Razzhivin, "Background subtraction in experimental data arrays illustrated by the example of Raman spectra and fluorescent gel electrophoresis patterns," *Instrum. Exp. Tech.* **46**(6), 765–769 (2003).
35. S. Sugio et al., "Crystal structure of human serum albumin at 2.5 Å resolution," *Protein Eng.* **12**(6), 439–446 (1999).
36. X. Peng et al., "Study on the structural changes of bovine serum albumin with effects on polydatin binding by a multitechnique approach," *Spectrochim. Acta, Part A* **81**, 209–214 (2011).
37. A. I. Ivanov et al., "Infrared and Raman spectroscopic studies of the structure of human serum albumin under various ligand loads," *J. Appl. Spectrosc.* **60**, 5–6 (1994).
38. C. Zhenhuan et al., "UV Resonance Raman-selective amide vibrational enhancement: quantitative methodology for determining protein secondary structure," *Biochemistry* **37**, 2854–2864 (1998).

Anastasiya S. Svetlakova graduated from the Faculty of Physics, Lomonosov Moscow State University in 2015. Her area of expertise is Raman spectroscopy of enzymes and nanoparticles.

Nikolay N. Brandt graduated and received his PhD degree from the Faculty of Physics, Lomonosov Moscow State University in 1998 and 2001, respectively. He is a participant of international research projects in Tokyo and Berlin. He is an associate professor at the Faculty of Physics, Lomonosov Moscow State University. His area of expertise is Raman, IR, and fluorescence spectroscopy of biological macromolecules aimed at the analysis of the relationship of conformational dynamics and functional activity.

Alexander V. Priezzhev graduated and received his PhD degree from the Faculty of Physics, Lomonosov Moscow State University in 1971 and 1975, respectively. He is a leader and participant of international research projects on medical physics and biomedical optics in USA, Germany, Finland, China, and Taiwan. He is head of the Laboratory of Laser Biomedical Photonics, Faculty of Physics and International Laser Center, Lomonosov Moscow State University. His areas of expertise include but is not limited by biomedical optics, light scattering diagnostics, physics and rheology of biological fluids.

Andrey Yu. Chikishev graduated and received his PhD and Dr.Sci. degrees from the Faculty of Physics, Lomonosov Moscow State University in 1982, 1986, and 2002, respectively. He is a leader and participant of international research projects on laser spectroscopy of biomolecules and organic molecules in the Netherlands, Germany, Japan, and Italy. He is head of the Laboratory of Laser Diagnostics of Biomolecules and Methods of Photonics in the Study of Objects of Cultural Heritage, International Laser Center, Lomonosov Moscow State University.